Selected Applications of Planar Imaging Velocimetry in Combustion Test Facilities

Christian Willert[1], Guido Stockhausen[1], Melanie Voges[1], Joachim Klinner[1], Richard Schodl[1], Christoph Hassa[1], Bruno Schürmans[2], and Felix Güthe[2]

[1] Institute of Propulsion Technology, German Aerospace Center (DLR), 51170 Köln, Germany
chris.willert@dlr.de
[2] ALSTOM, 5401 Baden, Switzerland
bruno.schuermans@power.alstom.com

Abstract. This chapter provides an overview on the application of particle image velocimetry (PIV) and Doppler global velocimetry (DGV) in combustion test facilities that are operated at pressures of up to 10 bar. Emphasis is placed on the experimental aspects of each application rather than the interpretation of the acquired flow-field data because many of the encountered problems and chosen solution strategies are unique to this area of velocimetry application. In particular, imaging configurations, seeding techniques, data-acquisition strategies as well as pre- and postprocessing methodologies are outlined.

1 Introduction

Aeroengines as well as stationary power generation will continue to rely heavily on fossil and substitute fuels in the coming decades. Increasing fuel costs demand higher efficiencies, while new governmental regulations require a further reduction of emissions. The development of modern aeropropulsion and gas-turbine technology increasingly relies on combustion-related research projects that are driven by similar motivations, namely to provide experimental data to validate advanced simulation methods that model the extremely complex flows found in modern combustors. To offer a reliable alternative to expensive full-scale rig tests, confidence in numerical models has to be gained on the basis of validation experiments that capture certain aspects of the flow where a corresponding physical model is tested in isolation. In order to judge the performance of computational fluid dynamics (CFD) tools in realistic applications, data must also be obtained from facilities that are capable of capturing the rather comprehensive range of effects found inside the combustion chamber in relevant geometries and at higher pressures. The complexity and operational cost of full-scale combustor sectors prevents the application of advanced optical measurement techniques to fully capture the range of phenomena, such that compromises must be made by using simplified and/or downsized combustors.

On the other side, combustion CFD codes that are currently used in the design of combustors are based on Reynolds-averaged Navier–Stokes (RANS)

A. Schroeder, C. E. Willert (Eds.): Particle Image Velocimetry,
Topics Appl. Physics **112**, 283–309 (2008)

equations and rely on a steady-state solution of time-averaged flow equations. Although these codes have proven themselves valuable in the design process, the RANS approach has well-known deficiencies in accurately predicting features of turbulent flows like the spreading and mixing of turbulent jets, highly turbulent and genuinely unsteady flows. A more accurate prediction of the detailed flow and temperature field and distributions of chemical species will result in higher-accuracy predictions of emissions (NO_x, CO, unburned hydrocarbons, etc.). Some of the limitations of RANS codes can be overcome by the large eddy simulation (LES) method, where time-dependent turbulent fluctuations of a size larger than the size of the numerical grid are resolved accurately in time.

Confidence in improved CFD techniques cannot be solely built on validation experiments that represent one aspect of the flow where the corresponding physical model is tested in isolation. To qualify the numerical codes for practical calculations, highly resolved experimental data must be obtained from test facilities capable of presenting a rather comprehensive range of effects found inside the combustion chamber in relevant geometries and at higher pressure. In practice, these test facilities should represent the conventional combustor architecture with a diffusion burning primary zone, a mixing zone with colliding jets and film-cooled liner walls.

While spectroscopic methods are generally used for acquisition of temperature, mixture fraction and species data, velocity data obtained by laser Doppler velocimetry, PIV and DGV provides insights into the kinetic effects influencing the combustion processes, especially under the influence of increased pressure or combustion oscillations.

This chapter intends to summarize experiences gained in bringing both PIV and DGV to (routine) application on combustion test facilities. While the experimental data obtained in these applications are described elsewhere with respect to their physical significance, the emphasis here is to give some background on the general solution strategies that led to the successful acquisition of this data.

2 Challenges on Diagnostics

A successful application of both PIV as well as DGV in combustion facilities depends on a careful optimization of three equally important issues: 1. optical access, 2. imaging aspects and 3. seeding techniques. In the following, each of these three aspects are briefly described with particular emphasis on PIV.

2.1 Optical Access

Clearly, any optical diagnostic method, be it of pointwise (e.g., LDA, PDA, Raman scattering) or planar (e.g., LIF, PIV, DGV) nature, requires adequate optical access to the generally confined flow of the combustion test facility.

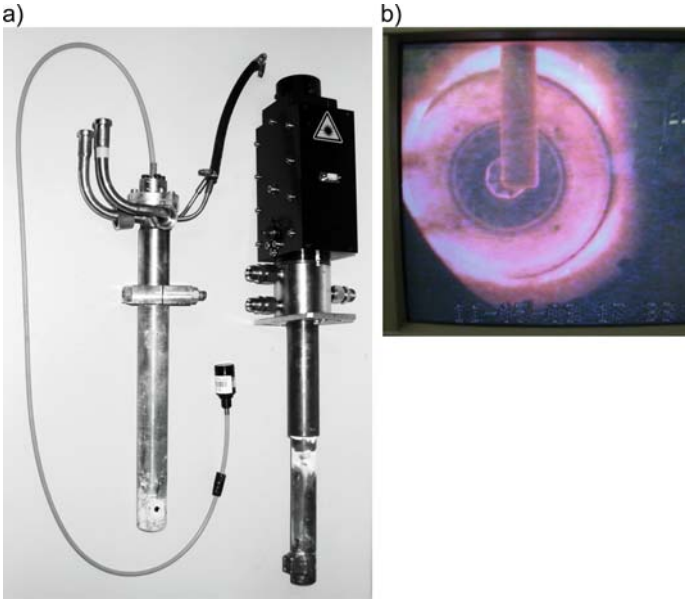

Fig. 1. (**a**) Water-cooled imaging fiber periscope (*left*) and lightsheet generator probe (*right*) used for DGV in combustors; (**b**) video image of an imaging periscope mounted about 0.7 m downstream of a gas-turbine combustor

In the case of PIV a laser lightsheet has to be introduced that is observed by the imaging optics of a recording camera. While periscope probes as shown in Fig. 1 are feasible for the introduction of the lightsheet into the facility, the rather low resolution of imaging periscopes may allow intensity-based DGV measurements, as this technique does not require that particles are discretely resolved. However, the low optical resolving power of these imaging periscopes is unsuited for PIV imaging. So, in practice at least, one viewing window is required to properly resolve particles suspended in the flow.

However, these windows must also sustain high temperatures as well as elevated pressures that often results in rather complex designs consisting of multiple windows (thin liner window combined with thick pressure window). Active film cooling is frequently used to protect the window from the high temperatures near the reaction zone with the drawback that the cooling film may influence the reaction processes. A close collaboration between the facility designers, combustion experts and optical measurement specialists is of utmost importance during the design phase of the facility to ensure a reasonable balance between adequate optical access and its possible influence on the flow physics.

2.2 Imaging Aspects

Figure 2 shows a PIV recording obtained from a kerosene flame inside a single-sector combustor and illustrates a number of issues that are representative of the application of PIV to combustion facilities. Here, the lightsheet plane is parallel to the centerline of the double-swirl fuel nozzle that itself is hidden from view at the lower edge of the image. The lower portion of the image shows a cross section through the kerosene spray cone that is ejected from the nozzle and contains areas of significant overexposure of the CCD sensor as exhibited by saturated pixels. The vertical stripes in these overexposed areas result from pixel blooming on the CCD sensor – the high-intensity signal spreads the overflowing charge into neighboring pixels. This overexposure is caused by the rather large droplets (typically $\geq 50\,\mu\text{m}$) for which the scattering cross section is significantly larger than for the micrometer-sized flow seeding for which the PIV recording system is optimized. The problem is limited to the lower half of the image since the droplets evaporate as they propagate upward into the flame. In order to distinguish droplet velocity from gas velocity of this two-phase flow various strategies are possible. In the present case, highpass filtering combined with binarization of the acquired images matched the intensity levels of the seeding with that of the kerosene droplets such that areas normally biased to the velocity of the kerosene droplets could be corrected in favor of the gas velocity [1]. The image-enhancement procedures and their effect on the recovered displacement data are illustrated in Fig. 3. An alternative approach using the fluorescence of both particles and fuel was proposed and applied by *Kosiwczuk* et al. [2, 3]. However, the applicability of the technique to pressurized combustion has yet to be tested with regard to stability of the fluorescent dyes at higher temperatures.

The sensor saturation in the upper half of the image of Fig. 2 has a different cause: this is the region of highest flame luminosity that cannot always be removed solely through the use of a laser line filter. As illustrated in Fig. 2c the signal levels in this area differ significantly between the frames of the image pair (1500 vs. 4000 counts) that results from the fact that the second frame of current PIV cameras stays sensitive for the time required for the readout of the previously recorded first-image frame. This readout time is on the order of 50–100 ms compared to less than 1 ms for the first frame. Flames with high fuel-to-air ratios at elevated pressures are characterized by strong luminosity (e.g., glowing soot) such that narrow-banded laser line filters are not always sufficient for its suppression. A solution to this problem could be the use of a pair of CCD cameras – each individually shuttered electronically – with a common viewing axis [4]. A more practical solution is the use of mechanical or electro-optic shutters. While mechanical shutters provide complete extinction, their lifetime is limited when operated at high frame rates and steep rise/fall times. Electro-optic shutters have rise times in the submicrosecond range but either have low transmission ($< 40\,\%$) as

for ferroelectric devices [5] or have low extinction ratios as for liquid crystal scattering shutters [1].

The recording shown in Fig. 2 contains a third problem that is not immediately obvious: Even in the absence of both flame luminosity and particulate seeding there is significant background illumination that not only lowers the overall contrast but may even result in a complete loss of signal due to sensor saturation. This background lighting is primarily caused by laser light scattered from window surfaces and illuminates features within the field of view such as the circular port in the background of Fig. 2a. The undesired signal generally increases during facility operation due to the increased deposition of seeding on the windows. The use of light traps and recessed windows reduces the problems [6] but is not always possible on a given facility. Aside from the saturation of the sensor, measurements close to windows are difficult due to the stationary speckle signal resulting from light scattered by the deposited seeding.

Image quality in terms of resolution ultimately depends on the integral distortion effects between the individual light-scattering particle and the imaging sensor. The use of high-quality recording lenses and plain quartz glass windows is generally sufficient in isothermal PIV applications. Temperature gradients inside and outside of combustion facilities introduce light refraction along the imaging path that results in both the displacement of the particle image on the sensor (similar to background-oriented Schlieren, BOS) and, even worse, a blurring of the particle image. This beam-steering effect also strongly affects other point-resolving techniques such as laser/phase Doppler anemometry (LDA, PDA) as well as spectroscopic techniques such as Raman scattering. The blurring can be roughly considered as a sum or product of temperature, pressure and penetration depth, such that the application of PIV may fail with increasing facility size and operating pressures. Blurring can be controlled to some degree by two simple techniques. First, an increased distance between the recording lens and the optically disturbed media (by using zoom lenses) reduces beam steering, which is similar to reducing the sensitivity in a Schlieren setup. Secondly, a reduced lens aperture confines the light-collecting cone such that all light rays pass similar refracting media resulting in a sharper image. This is particularly useful for highly turbulent flows with locally strong modulations of density. The disadvantage of this approach is the increased depth of field that may bring (grainy) areas into focus that disturb the PIV correlation signal (e.g., seeding deposits on windows or walls).

2.3 Seeding of High-Temperature, Reacting Gas Flows

Aerosol seeding using atomized liquids, which is common in many aerodynamic applications, is not possible in high-temperature reacting flows due to evaporation and/or combustion of the droplets. In these cases, seeding based on solids must be used. Metal oxide powders are especially well suited for

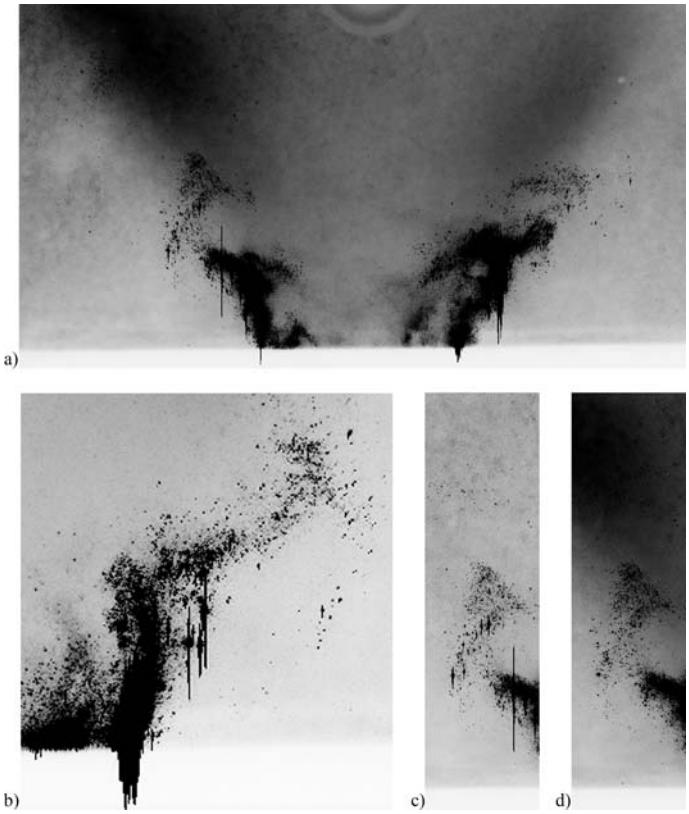

Fig. 2. PIV recording of kerosene flame above a double-swirled fuel nozzle at 3 bar (to enhance contrast, the negative image is shown: *black areas* are brightest), (**b**) detail of the kerosene fuel spray exhibiting strong saturation of sensor, (**c, d**) corresponding regions from each frame showing effects of flame luminosity

this purpose due to their inertness, high melting point and rather low cost. Titanium dioxide, alumina and silica powders are some of the most commonly used materials. However, the controlled dispersion of these powders is more challenging than for liquid materials since the powders have a strong tendency to form agglomerates, especially for small grain sizes in the submicrometer range. Therefore, the seeding device has to either break up the agglomerates or remove them from the powdered aerosol prior to delivery into the facility such as through the use of a cyclone separator [7, 8].

Another approach to deagglomerate the bulk seed material was proposed by *Wernet* and *Wernet* [9]: the interparticle forces responsible for the agglomeration can be directly influenced by controlling the acidity of liquid suspensions of the seed material. They suggest the use of acidic (pH $\sim$ 1) dispersions of alumina/water or alumina/ethanol that can be dispersed us-

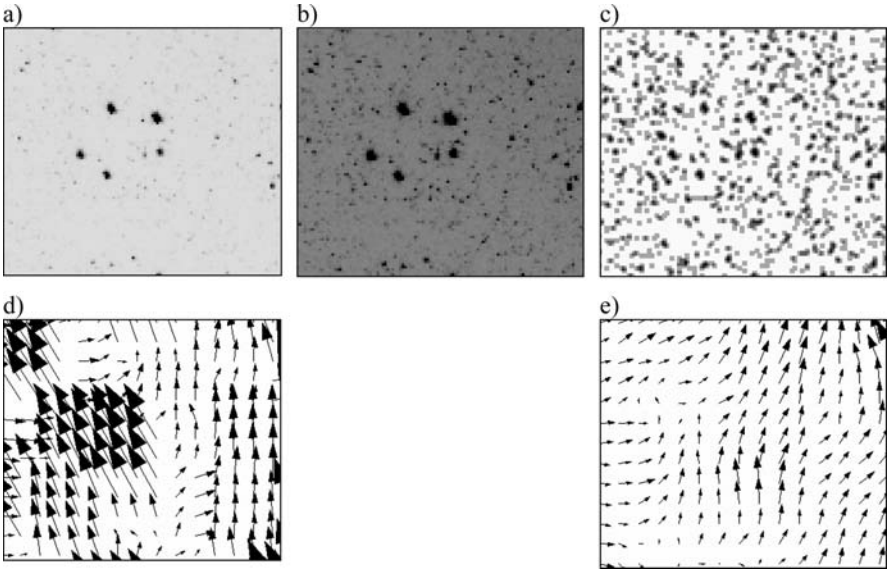

Fig. 3. Portion of PIV recordings – inverted for clarity – and processed PIV data: (**a**) fuel droplets, (**b**) brightened version of (a) with seeding visible, (**c**) preprocessed image, (**d**) flow field after standard PIV analysis, (**e**) flow field obtained after enhancement of PIV images, (from [1])

ing liquid atomization. The solid seed material remains after evaporation of the carrier liquid.

Depending on the relative mass-flow rates between seeded and unseeded flows the use of liquid-particle suspensions is not always feasible, especially when the flow may be disturbed due to evaporation cooling and/or changes in the reactive chemistry. Therefore, the aerosol should be created through dispersion of the dry powder. A common approach is to aerate the powder inside a vertical tube from below, resulting in a so-called fluidized bed. The flow rate through the seeder is chosen just large enough such that the bed of particles is fluidized, carrying smaller particles into the region above the bed (known as the freeboard) toward the exit orifice and from there into the facility under investigation. Figure 4 shows a simple fluidized-bed seeding device for use in elevated-pressure applications [1, 10]. This generator has two noteworthy features: the strong shear flow present in a sonic orifice at the exit breaks up larger agglomerates. The size of this orifice is chosen to ensure sufficient flow rate to aerate the powder. The second feature is a bypass line that can be used to maintain constant mass flow rates into a test facility even when no seeding is required.

The following gives some recommendations for the successful operation of fluidized-bed seeders:

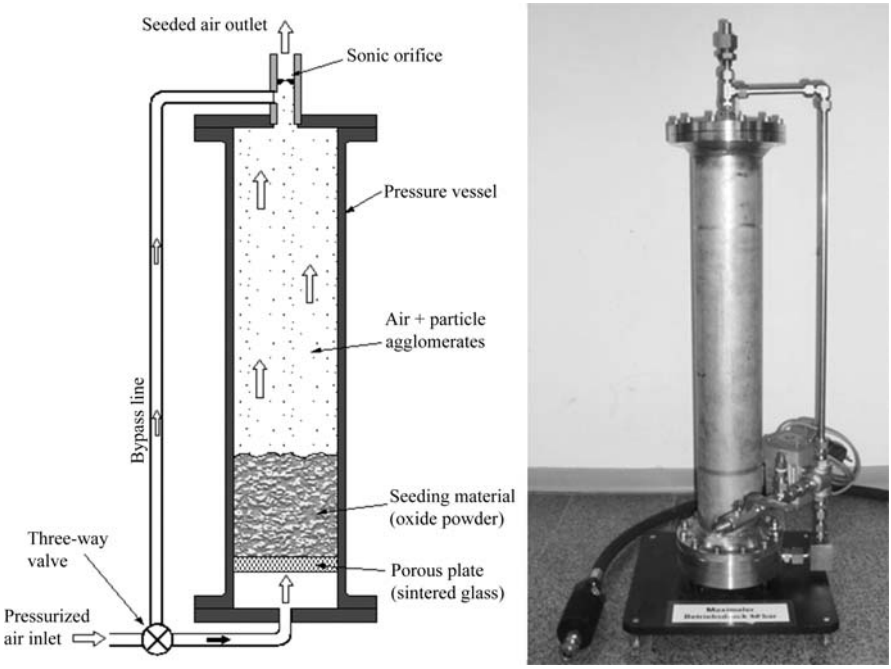

Fig. 4. Fluidized-bed seeding device for high-pressure applications

- The seeding powder should be kept dry, preferably by heating the material to remove excess moisture before filling the seeding device. Dry air or nitrogen should be used to operate the seeder.
- Short supply lines between seeder and facility should be used to prevent the formation of agglomerates. If possible, additional carrier air should be used to reduce the relative seeding concentrations.
- Frequent agitation of the seeding system reduces the chance of channel formation within the fluidized bed.
- The mechanical interaction of the seed material with small brass spheres (100–500 µm) added to the fluidized bed also helps to break up agglomerates. This configuration is referred to as a two-phase fluidized bed.

In the various applications described herein the fluidized-bed seeding generator was operated using mainly alumina particles (Al_2O_3). Operation of the seeder was not always reproducible, which in part could be attributed to moisture in the carrier air stream. Although the manufacturer had specified a mean particle size in the 0.8 µm range, scanning electron microscopy (SEM) of the powder revealed the presence of a significant number of very small particles in the 100–300 nm range (Fig. 5). Particles of this size have very low light scattering (Rayleigh scattering) and are considered to be unsuitable

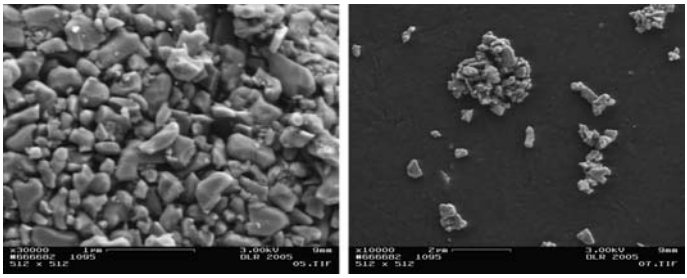

Fig. 5. Micrographs of alumina powder (Martinswerk, Martoxid MR70) used in the presented PIV applications (Images courtesy of R. Borath, DLR Institute of Materials Research, Köln)

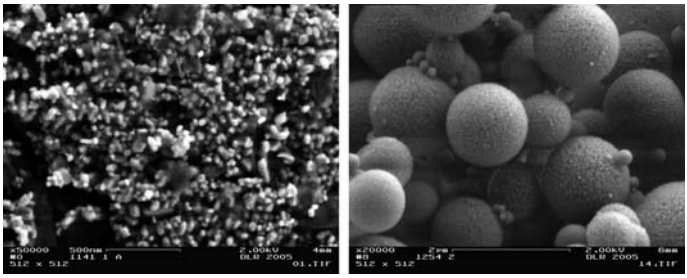

Fig. 6. Micrographs of titanium dioxide (Kemira, UV Titan L830). *Right:* porous silica spheres for PIV seeding (Images courtesy of R. Borath, DLR Institute of Materials Research, Köln)

for PIV. It is believed that only a fraction of the particles are resolved by the PIV camera, while the bulk of the material adds to a mean background intensity and faster window contamination. These observations prompted a search for better seeding materials that offer a narrow size distribution in the 1 µm range. A few examples obtained during this search are shown in the SEM images of Fig. 6.

Titanium dioxide (TiO_2) particles are used rather frequently in velocimetry although their availability is limited to primary sizes in the 50–300 nm range (for color-enhancement demands). In supersonic-flow applications of PIV this material has been used successfully in conjunction with cyclone separators [7]. However, in combustion applications titanium dioxide was observed to drastically reduce in scattering signal within the reaction zone, which most likely can be attributed to a breakup of larger agglomerates into the primary size particles during the rapid thermal expansion in the reaction zone. This could not be observed with the alumina material used in the present applications.

Alternatively, silicon dioxide (SiO_2) particles are available as ground material or as spheres. Although more expensive than polydisperse particles, spherical monodisperse particles hold the biggest promise with regard to optimizing the tradeoff between facility contamination and signal yield. This was confirmed by preliminary atmospheric tests with this material. Other materials yet to be tested in a combustion environment are made of porous silica and have bulk specific weights as low as 0.1, which should produce very good aerodynamic properties (Fig. 6, right).

3 Sample Applications

With the exception of the previously described seeding device, rather standardized, commonly available PIV hardware was used for all applications that are described in the following sections. Illumination was provided by frequency-doubled, double-cavity Nd:YAG lasers (wavelength $\lambda = 532\,\text{nm}$) with an energy of 100–150 mJ per light pulse. An articulated light-guiding arm was generally used to improve overall handling and laser safety. PIV recordings were obtained using thermoelectrically cooled CCD cameras with resolutions of either 1280×1024 or 1600×1200 pixel. A laser line filter placed in front of the aperture of the photographic imaging lens was generally sufficient to suppress the flame luminosity. Table 1 summarizes the applications with regard to experimental aspects.

3.1 PIV in a Pressurized Single-Sector Combustor

Initial efforts of applying PIV in a pressurized combustor at the DLR Institute of Propulsion Technology date back to 2000 and were undertaken on a single-sector facility (SSC), shown in Fig. 7. With a rather small square cross section of $100 \times 100\,\text{mm}^2$ the facility is primarily used for the investigation of new burner designs using optical techniques, especially spectroscopy and velocimetry. Aside from good optical access from at least three sides, one advantage is that the facility can be traversed in all three directions, which greatly simplifies the use of optical diagnostics, even those with high setup complexity. The facility can be operated at up to 20 bar with mass flows up to 1.5 kg/s at 850 K preheating. The pressure and mass flow in the chamber is controlled through a sonic orifice at the exit. Jets in crossflow arrangement at a roughly midlength position of the 250-mm long combustor provide preheated mixing air and confine the primary zone to a roughly cubic volume.

Optical access is granted from three sides through windows consisting of a thick pressure window and a thin liner window. The gap between the windows is purged with cooling air, while the inside of the liner window is film cooled using a portion of the plenum air.

For PIV the lightsheet was aligned with the burner axis with the camera arranged in a typically normal viewing arrangement. By allowing the laser

Table 1. PIV parameters for the described combustion applications

		SSC1	GenRig	SSC2	Alstom
facility type		double annular swirl nozzle			swirl-stabilized premix burner
fuel		kerosene	gas	gas	gas
operating pressure	(bar)	3	atmospheric	2 and 10 bar	atmospheric
imaging setup		2C PIV	2C / 3C PIV	DGV-PIV	2C PIV
field of view	(mm^2)	100×50	85×110	100×60	200×250
recording lens	(mm)	55, $f_{\#}8$	55, $f_{\#}4$ 105, $f_{\#}4$	55, $f_{\#}2.8$	55, $f_{\#}4$
camera resolution	(pixel)	1280×1024	1200×1600	1280×1024	1600×1200
acquisition rate	(Hz)	≈ 2	15	≈ 2	15
laser pulse delay	(µs)	3	10	2	7
exposure time (1st frame)	(µs)	≈ 10	10	≈ 10	10
exposure time (2nd frame)	(ms)	≈ 120	≈ 33	≈ 120	≈ 33
acquisition mode		continuous	phase-resolved	continuous	phase-resolved
flame oscillation frequency	Hz	–	≈ 430	–	≈ 100–200
maximum velocity	(m/s)	≈ 70	≈ 50	≈ 120	n.a.
interrogation window size	(pixel)	32×32	48×48	32×32	64×64
spatial resolution	(mm^3)	$1 \times 1 \times 1$	$1 \times 1 \times 1$	$1 \times 1 \times 1$	$2 \times 2 \times 1$
images per sequence		13	188	100 (1000 for selected cases)	188
total acquired image pairs		≈ 500	≈ 29000	≈ 10000	≈ 25000
seeding material		SiO_2, 0.8 µm	Al_2O_3	Al_2O_3	Al_2O_3
reference		[1]	[11]	[10]	–

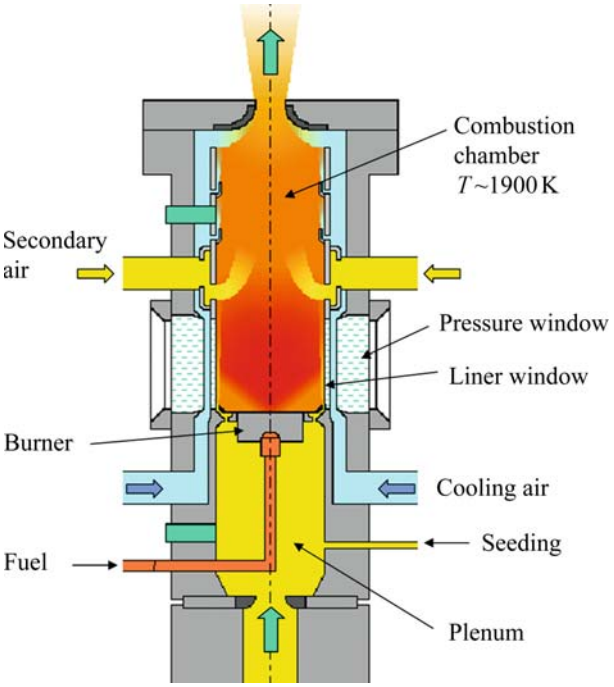

Fig. 7. Longitudinal cross section of the pressurized single-sector combustor (SSC)

lightsheet to pass straight through the combustor the amount of laser flare on imaging windows and walls could be kept at an acceptable level.

Seeding, consisting of amorphous SiO_2 particles, was introduced to the plenum upstream of the burner through a porous annular tube. As the window film cooling is supplied directly with seeded air from the plenum, the windows are unfortunately subjected to an accelerated buildup of seeding deposits. Preferably the film-cooling air should have been separated from the main burner air. Fired with kerosene the combustor provided PIV images of the type shown in Fig. 2, exhibiting strong Mie scattering off the kerosene spray as well as strong flame luminosity. A corresponding PIV result obtained for a slightly leaner operating condition with less kerosene spray is provided in Fig. 8. Image enhancement, as shown in Fig. 3, was applied prior to PIV processing and reduced the influence of droplet velocities on the air flow velocity estimates by equalizing the droplet image intensities with the much weaker intensity of the seeding particles [1].

3.2 Stereoscopic PIV in a Generic Gas Combustor

In order to gain further insights into the aerothermodynamical processes that govern the limit cycle of combustion driven oscillations frequently found in

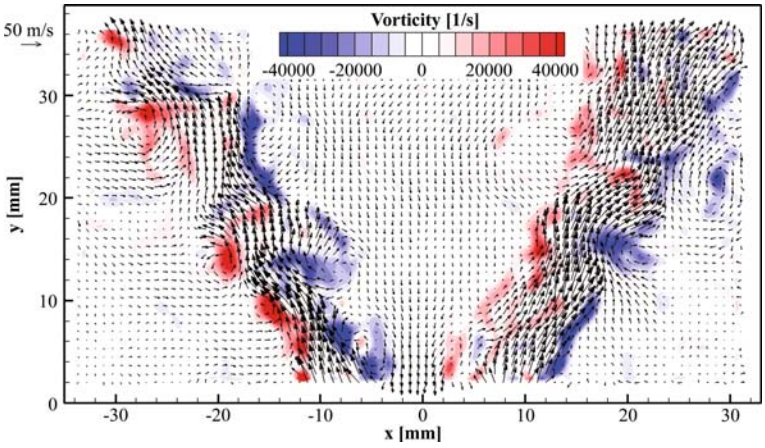

Fig. 8. Single PIV data set for the flow above a coswirled, kerosene air blast fuel nozzle operated at 3 bar obtained from the facility shown in Fig. 7

lean combustion systems a generic combustor was designed. The dynamics of the combustion process were influenced through a variation of preheat temperature, air mass flow/pressure drop over the burner and stoichiometry. The goal of the parameter variation was to find operation points with combustion-driven oscillation at realistic preheat temperatures and pressure drops over the burner. In the course of the project, phase-resolved measurements of the three-component velocity field were to be obtained by stereoscopic PIV (SPIV) measurements at specific points of operation.

The generic gas combustor (Fig. 9, left) consisted of a rectangular combustion chamber $85 \times 85 \times 114\,\mathrm{mm}^3$ in size with the double swirl nozzle centrally located at the bottom. The combustor offered optical access from three sides through thin (2 mm) quartz glass windows. The fourth, metal side wall contained thermocouples, a pressure sensor and an ignition unit. Two highly sensitive sound-pressure sensors were located in one corner pillar of the combustion chamber and provided acoustic signals associated with the combustion-driven oscillations (dominant frequency $\approx 430\,\mathrm{Hz}$). The filtered chamber-pressure signal obtained from these sensors was used to phaselock the PIV image acquisition.

The SPIV setup was optimized during a feasibility study prior to the measurement campaign in order to reduce direct laser-light reflections and scattered light to an acceptable minimum. In the final setup one camera was arranged in a classical (2C) normal viewing position combined with a second camera inclined to a 45° offaxis view, as shown in Fig. 10. One important advantage of this arrangement was that the entire chamber could be imaged in a classical 2C PIV setup that would not have been possible for symmetrically arranged stereo-PIV configurations. Figure 11 shows two PIV results

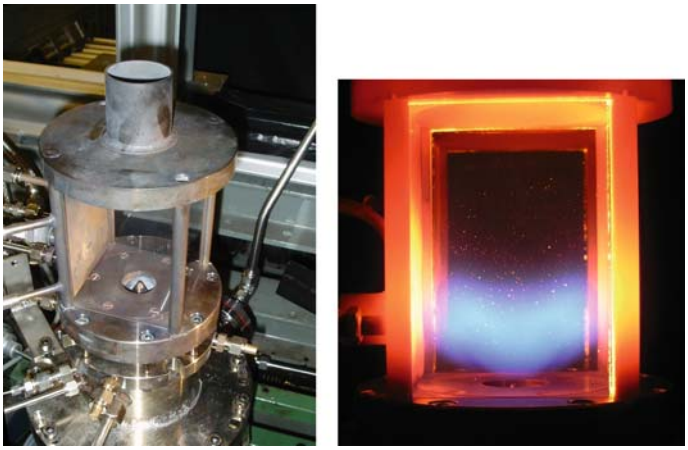

Fig. 9. Generic gas combustor (*left*) operating under atmospheric conditions (*right*)

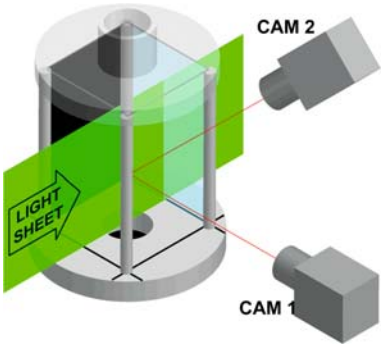

Fig. 10. Imaging configuration for stereoscopic PIV on small-scale generic model combustor

of phase-averaged 2C velocity fields acquired in the symmetry plane of the burner.

For the stereoscopic configuration the combined viewing area was restricted to the lower half of the combustor due to viewing obstruction caused by the lid of the chamber. Therefore, the 3C flow field could only be reconstructed for the lower half of the combustion chamber in the vicinity of the burner exit (see Fig. 12). As the entire PIV setup was installed on a three-axis traversing bench, different coplanar measurement planes could be acquired efficiently without requiring additional recalibration.

The PIV measurements were initially hampered due to strong temperature gradients outside the combustor, which were associated with density fluctuations and a natural convection in the surrounding air: This in turn led to significant optical blurring and displacement of the particle images, especially for the obliquely viewing camera – even though the imaging optics were already optimized for the minimization of these effects (e.g., long focal

lengths, reduced apertures). The problem could be solved effectively by forcing cooler ambient air into the imaging path outside of the burner by means of a blower. The combustion, its oscillation in particular, was not affected by this measure.

As the air-fuel ratio was the most sensitive parameter for the adjustment of the combustion-driven oscillation, the additional mass flow injected into the plenum upstream of the burner by the fluidized-bed seeding device had to be taken into consideration. To maintain a stable operating condition regardless of whether seeding was injected or not, the seeding device was operated continuously with a bypass line, allowing a supply of particles only when required (seeding duration $\approx 20\,\mathrm{s}$). Nonetheless, the lack of purging air on the windows resulted in unavoidable deposition of particles on the windows, which in turn limited the PIV acquisition to 3 to 5 sequences per burner test run. Here, the higher acquisition rate of the current camera systems (15 Hz) was a clear advantage, resulting in 200 images per sequence within 13 s.

The most challenging part of the stereo-PIV processing was the treatment of the stray light scattered from the chamber base plate, which illuminated the image background of the oblique view camera. Laser flare on the metal surface of the nozzle could not be avoided nor suppressed with laser line filters and/or background image subtraction during postprocessing. This resulted in a loss of signal in these areas. Consequentially, the affected image region had to be masked, as is visible in Fig. 12. This problem is representative of the application of stereo-PIV in confined facilities in general where the necessary oblique viewing arrangement causes additional flare regions on the imaged area either from windows or other surfaces that normally can be avoided in classical 2C imaging arrangements. As will be described in a different application later, the combination of PIV with DGV can partially alleviate this problem by relying on a single (lightsheet-normal) viewing direction only.

3.3 Phase-Resolved Measurements of a Gas-Turbine Combustor

In this application, the heat release and flow field of a gas-turbine burner was studied using phaselocked PIV and OH-chemiluminescence. Here as well, the aim of the experiments was to obtain a better understanding of thermoacoustic interactions in the combustion process. Therefore, the interaction between heat-release fluctuations, acoustic fluctuations and velocity/vorticity fluctuations in the combustion process was investigated experimentally.

The atmospheric test facility consisted of a single swirl-stabilized burner that issued into a combustion chamber of $380 \times 280\,\mathrm{mm}^2$ cross section. The experimental configuration, shown in Fig. 13, employed a standard, two-component PIV imaging arrangement with the laser lightsheet introduced to the facility through a narrow window at the bottom. The camera observed the flow immediately downstream of the nozzle in the axial symmetry plane of the burner. A rather large ($\sim 220 \times 250\,\mathrm{mm}^2$), air-film-cooled, viewing window provided optical access to most of the cross section. Seeding was

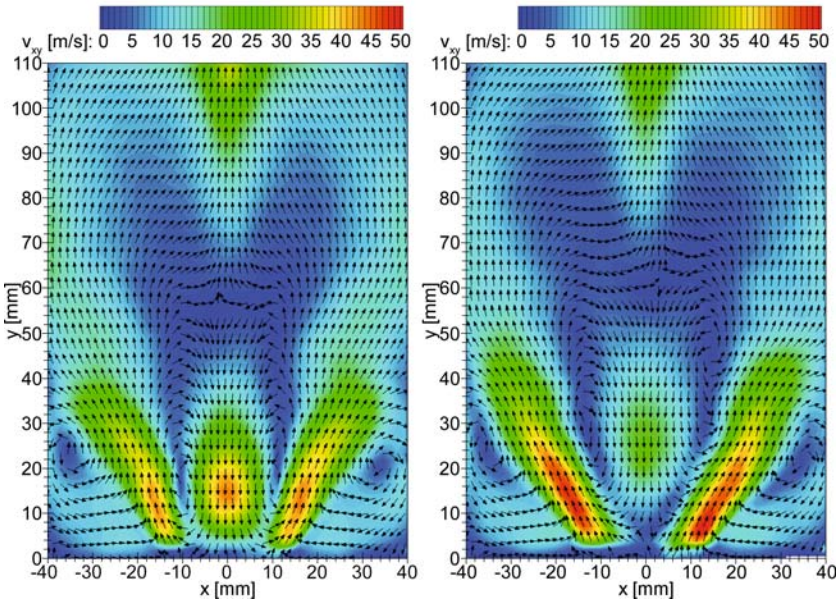

Fig. 11. Phase-resolved, two-component PIV results obtained at the symmetry plane (*color coding* represents inplane velocity magnitude, *vectors* indicate flow direction only)

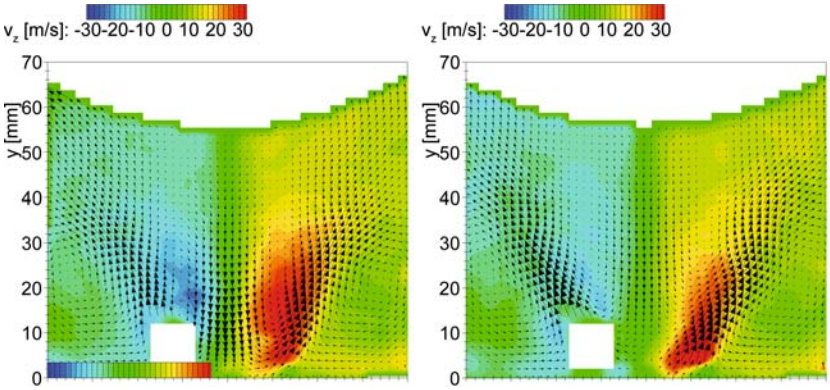

Fig. 12. Phase-resolved, stereoscopic PIV results at two different phase angles (color coding represents out-of-plane velocity)

provided by a pair of fluidized-bed particle seeders (Fig. 4) and was injected in the main flow upstream of the burner using a perforated annular tube. Due to the high mass flow rates in the facility two particle generators were used in parallel and supplied with dry, compressed nitrogen (1 % of total mass flow) to prevent possible clumping of the seeding powder.

As in the previously described application, the PIV camera and laser could be operated at 15 Hz repetition rate acquiring sequences of 190 images each ($\approx$ 12.6 s). Although the seeders were operated in a bypass mode for most of the time except for PIV acquisition, accumulation of seeding on the imaging window limited the data yield to about 10 useful PIV sequences before the system had to be shut down for window cleaning. This problem was compounded by the fact that the lightsheet directly hit the opposite wall, thereby illuminating the entire facility and especially that background area viewed by the camera. Clearly, an additional window for the passage of the lightsheet would have been advantageous here but was avoided in order to maximize the hot liner surface area that is known to have a direct influence on the combustion.

Because of the rather short operational times as well as the unsteadiness of the combustion oscillations (dominant frequency $\approx$ 100–200 Hz) at certain critical points of operation, the idea of acquiring phase-resolved data directly was abandoned in favor of a novel phaselocking method that allowed phase sorting of the PIV (and chemiluminescence) data in a postprocessing step (Fig. 14, 15). This was made possible by simultaneously recording a sound-pressure signal from the combustion chamber alongside with the PIV image acquisition instances on synchronized data tracks. The so-called Hilbert-Huang transform method (HHT) allows a decomposition of the sound pressure signal into instantaneous phase and frequency signals such that each individual PIV recording can be associated with a certain phase angle (and frequency).

The offline phaselocking method makes use of simultaneously recorded time traces of both the pressure signal and the camera (or laser) trigger signals as described in [12]. First, a bandpassed Hilbert transform of the microphone signal is calculated. The phase of this complex-valued time trace represents the instantaneous phase of the acoustic signal within the frequency band of interest. Because the filtering procedure is done offline, zero phase distortion can be achieved for the bandpass filtering operation. As the time instance of acquisition for each PIV image is available from the time trace, each image can then be assigned with an instantaneous phase for one (or more) frequency bands. Phase sorting and subsequent averaging of the instantaneous PIV data is performed across a number of equally spaced phase intervals (typically 8). Finally, the averaged images for each phase interval yield the phaselocked sequence. Because the phaselocking is done offline, the method is not restricted to the calculation of mean values at each phase angle. An additional advantage of this method is that the dynamic behavior

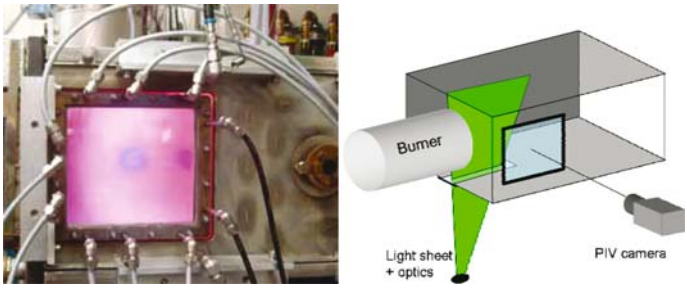

Fig. 13. Imaging window used for PIV measurements immediately downstream of a full-scale gas-turbine combustor

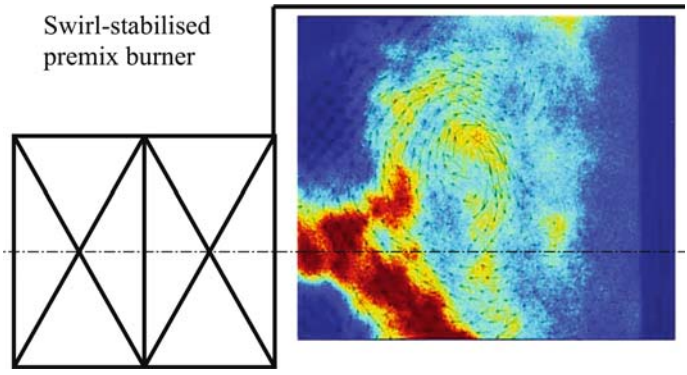

Fig. 14. Single-shot PIV data overlayed on a simultaneously acquired chemiluminescence signal (pseudocolored)

at several frequencies can be obtained from one experiment, which is not possible with standard phase-averaging methods.

In the present case the processed instantaneous PIV datasets were conditionally averaged for phase angle ranges of $\pm 22.5°$. Histograms of the phase distribution showed 15–30 samples per bin. The averaged velocity fields were then decomposed into their solenoid and irrotational parts. The unsteady solenoid part represents the fluctuating vorticity field, the irrotational part represents the acoustic motion. This, together with the chemiluminescence data – which correlates with the heat-release rate – allowed the analysis of thermoacoustic interactions at various operating conditions.

The postprocessed phaselocked results show the velocity field's fluctuation with respect to phase angle for the dominant frequency. Quantities such as the velocity components, the root mean square of the velocity vector, the magnitude of velocity and the curl of the velocity vector field (i.e., out-of-plane vorticity component) can then be derived. The unsteady part of all the aforementioned quantities is also found by subtracting the total mean

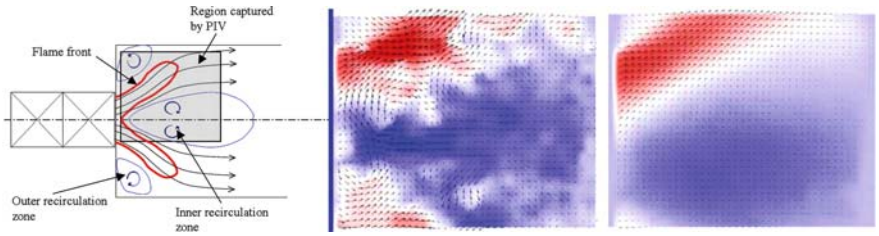

Fig. 15. Instantaneous and ensemble-averaged velocity maps obtained with PIV (*color coding* represents the horizontal velocity component)

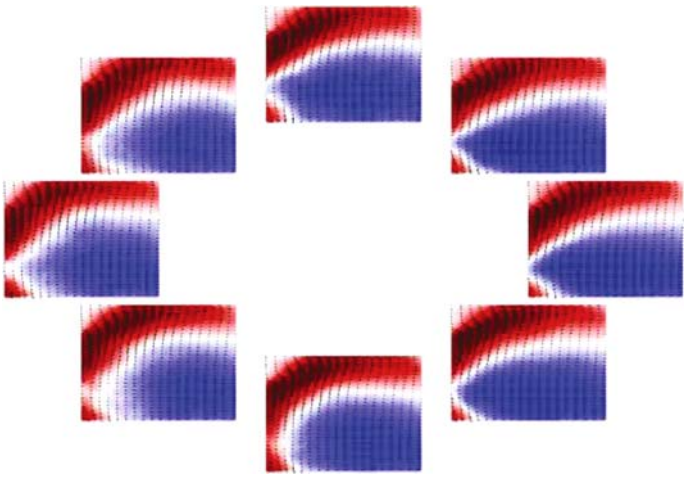

Fig. 16. Phase-resolved mean velocity maps obtained with PIV (*color coding* represents the axial velocity component). Note the movement of the vortex stagnation point

from each phaselocked average. The axial velocity and the unsteady axial velocity are shown, respectively, in Figs. 16 and 17. The arrows represent the velocity fields, the colors indicate the axial component of the velocity. The white-colored region indicates an axial velocity of zero, the blue a negative axial velocity and the red a positive axial velocity.

For a given burner operating condition each PIV data series was decomposed into its rotational and irrotational velocity components prior to performing the phase averaging. The phase-resolved total component of axial velocity is shown in Fig. 16, and the unsteady picture is shown in Fig. 17. The unsteady part is representative of the acoustic motion of the fluid. So, it is not surprising to see a predominantly axial motion in Fig. 16, since the frequency of oscillation was well below the acoustic cuton frequency of the combustion chamber. This is also visualized by a phase-dependent movement

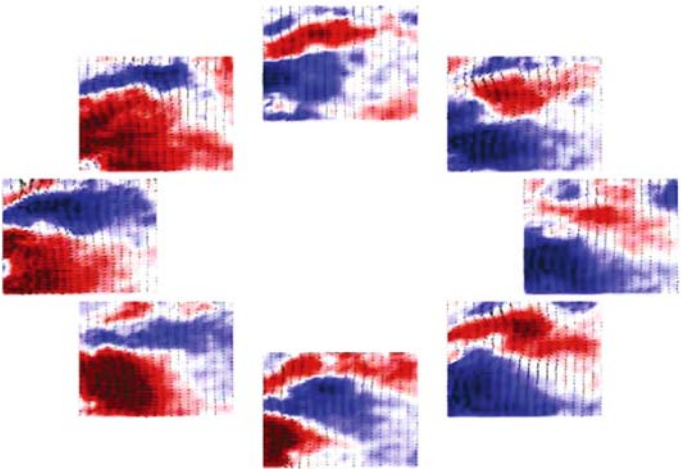

Fig. 17. Unsteady velocity data corresponding to the phase-resolved data shown in Fig. 16. (*color coding* represents the axial, horizontal, velocity component)

of the stagnation point. However, the gradient of the acoustic velocity is much larger than what would be expected based on the acoustic wavelength for this frequency of oscillation. This can be explained by analyzing the chemiluminesence data: it is found that the unsteady heat release is responsible for the gradients of velocity.

Further examples of the application of the Hilbert-Huang transform method to combustion research are described in [12]. In general the HHT method is applicable to essentially any type of randomly sampled experimental data for which a continuous time trace is available [13, 14].

3.4 Combined DGV and PIV in a Pressurized Gas-Turbine Combustor

The following planar velocimetry measurements were performed on the pressurized single-sector combustor facility (SSC) described in Sect. 3.1. The overall aim of the underlying project was to provide a comprehensive data set for validation of RANS and LES codes at isothermal as well as combusting conditions at 2 and 10 bar with 650 K preheat using natural gas as fuel [15]. While part of the investigation was focused on the primary zone, additional data was also to be provided of the secondary – or mixing – zone. This required a new combustor with optical access to the secondary zone as outlined in Figure 18. Due to the presence of mixing-air supply ports, optical access could only be facilitated by two windows facing each other. To, nonetheless, introduce a lightsheet parallel to the imaging windows, the new rig was additionally fitted with two narrow windows next to the burner's exit nozzle. In a first series of measurements the isothermal flow in planes parallel to the wall

with the mixing-air jet orifices could be measured using a stereoscopic PIV setup. However, with increased distance from the wall the coincident region as observed by both cameras was limited due to optical obstruction. In order to obtain a nearly complete picture of the flow field in the mixing zone, a combination of PIV with DGV was chosen.

Following Fig. 19 it is possible to reconstruct all three velocity components from a single viewing direction and single lightsheet: While PIV essentially provides the inplane velocity components, DGV measures the component projected on the bisector between observation and lightsheet vector. A straightforward vector transformation reconstructs the Cartesian velocity components from the three measured velocity components. The combined technique is very attractive as it considerably reduces the complexity regarding optical access (one view and one lightsheet). This concept was first successfully demonstrated by *Wernet* on a free jet using pulsed DGV together with PIV [15].

In the present application inside the combustor, a combination of DGV and PIV was chosen that is slightly different from the one presented by *Wernet* [16] since a suitable, frequency-stabilized laser for pulsed DGV was not available. Here, it was necessary to apply PIV and DGV in succession.

The current limitation of the combined PIV-DGV technique presented here is that the DGV laser system and camera was designed for acquisition of time- or phase-averaged velocity data [6,17]. While the PIV measurements inherently provide unsteady velocity data, DGV images are obtained through on-camera integration of many pulses (at least 1000) of scattered light from a laser with rather low pulse energy ($\approx 2\,\mathrm{mJ}$, [6]). This means that information regarding temporal fluctuations is lost during acquisition of the DGV images. Nevertheless the corresponding PIV data sets can at least provide two components of the fluctuating data but should also be treated with caution since 100 images acquired for each plane as in the present case are insufficient to properly estimate the fluctuating components.

The utilized PIV hardware and seeding approach was equivalent to that of the previously described applications. The lightsheet was introduced through one of the narrow windows of the combustor's exit flange and aligned orthogonally to the viewing direction of the PIV camera. The unique capability of traversing the combustor rig with respect to a stationary optical diagnostic setup allowed the efficient acquisition of the multiple coplanar datasets by PIV and DGV, thereby mapping a complete volume of the flow field with three velocity components.

Data acquisition took place in two phases, first acquiring a volumetric PIV dataset, followed by exchange of hardware and subsequent acquisition of the corresponding DGV frequency shift images under equivalent operation conditions and corresponding spatial positions. In total, 41 coplanar slices of combined DGV-PIV data were acquired, resulting in a volumetric dataset of time-averaged, three-component velocity measurements as shown in Fig. 20. The spatial resolution of the velocity data is roughly $1 \times 1 \times 2\,\mathrm{mm}^3$. The

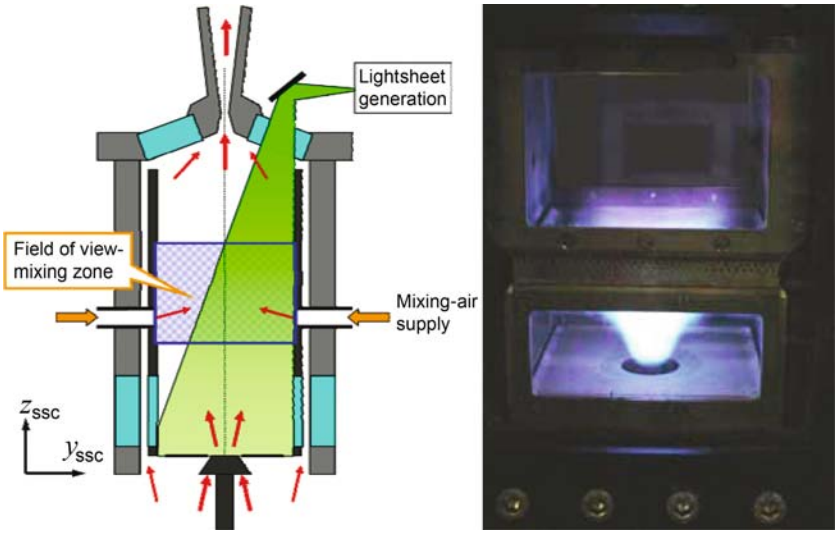

Fig. 18. Imaging arrangement used for mapping of the flow in the mixing zone by means of combined DGV and PIV. *Right:* photograph of the flame at a pressure of 4 bar and air preheating temperature of 700 K

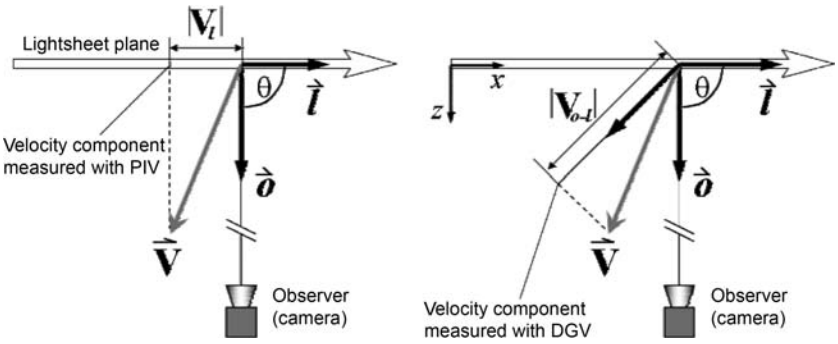

Fig. 19. Combination of PIV with DGV can be used to recover the out-of-plane velocity component from a single viewing direction (from [10])

influence of the mixing jets up until the middle of the combustor is clearly visible in Fig. 20b. The mixing jets also limit the recirculation region, as indicated by the abrupt change of the vertical velocity component displayed in Fig. 20c. Further details about this application and its results can be found in [10] as well as [15].

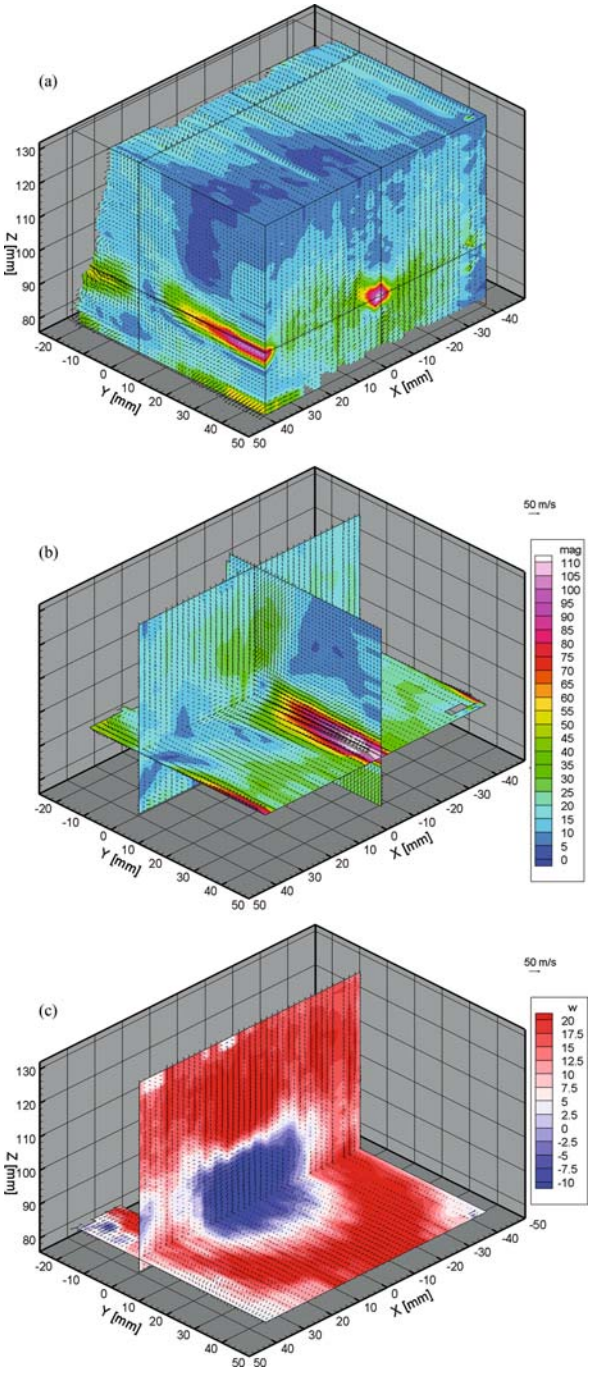

Fig. 20. Volumetric time-averaged velocity dataset of the mixing zone obtained at 2 bar (from [10])

4 Conclusions

As exemplified by the four previously described applications, the development and qualification of planar velocimetry (PIV and DGV) for use in combustion test facilities has undergone significant progress in the past 6 years, taking profit not only from technological advances in PIV as a whole, but also through a better understanding of the problems specific to this particular range of applications. In particular, seeding techniques, relying on the dispersion of powdered, noncombusting solid particles, have been improved sufficiently to allow seeding of significant mass flows ($\geq 1\,\mathrm{kg/s}$) at elevated pressures (up to 20 bar). Further investigations in this area are still in progress to improve the continuity of the particle dispersion and to develop strategies that limit the undesired accumulation of seeding deposits in the facility, especially on the windows. Here, a close collaboration between the facility designers and optical metrology personnel is mandatory during the design phase of new test facilities to allow, for instance, the introduction of seeding only to relevant areas in the facility that leave window-cooling films unseeded.

Nonetheless, a gradual accumulation of seeding deposits in the facilities can not be avoided entirely. These deposits increase light scattering from normally matte surfaces (e.g., combustor liner walls) and may result in a loss of signal for PIV due to saturation of the sensor. This stray light may also constitute a significant error source in intensity-based imaging techniques such as DGV since it cannot be separated from the desired signal by *a-priori* measurements in the absence of seeding. One recently proposed solution to this problem essentially relies on estimating the background luminosity from additional DGV images of a striped (spatially intensity modulated) light-sheet [18]. With this correction method it was then possible to rectify a velocity bias exceeding 30 m/s of a flow field measured inside a large-scale combustor facility.

The described problems associated with increased Mie scattering off large fuel droplets may be less of an issue in future measurement campaigns as new burner designs increasingly utilize premixing and pre-evaporation of liquid fuels for improved combustion. Nonetheless, approaches based on fluorescence imaging can allow a nearly complete separation of the two-phase flow in gas velocity and droplet velocity fields. One such approach has been recently suggested by *Kosiwczuk* et al. [2,3] and relies on the different fluorescence signals of the fuel and particles that are captured by two cameras with different color sensitivity. The applicability of the technique to pressurized facilities depends on the stability of the fluorescence molecules at elevated temperatures and pressures.

While new approaches are being developed to improve the applicability of both DGV and PIV to combustion flows, the rapid technological development of lasers, camera hardware and imaging tools is of immediate benefit for the application of these techniques. Faster cameras and lasers enable higher

image acquisition rates and are less influenced by flame luminosity due to the reduced digitalization time of the images. Increased frame rates (can) reduce facility operating costs and may eventually make time-resolved measurements of the velocity field possible, thus allowing unsteady phenomena to be captured, for example, flame-out and reignition processes during lean-combustor operation.

In parallel with the continuous hardware advance, there is also an immediate need to improve data processing, data handling and subsequent postprocessing techniques and archival. The vast amount of PIV image data acquired in rather short times, often with marginal signal-to-noise ratios, has to be processed efficiently and preferably without too much user intervention. While the recent literature reports considerable advances in improving the precision of PIV image processing, there is still significant work to be done toward faster, self-optimizing PIV algorithms capable of delivering data with reliable quality estimates. Of course this requirement by no means is restricted to the previously described field of application, but is of significant importance for widespread future utilization of PIV in industry and research alike.

Acknowledgements

Portions of the presented material were produced in the framework of the following European Community research projects:

MOLECULES "Modelling of Low-Emission Combustors Using Large Eddy Simulations" funded under the "Competitive and Sustainable Growth" Programme, Contract N: G4RD/CT 2000/00 402.

FUELCHIEF "Demonstration of a Low NOx Fuel-staged Combustor in a High Efficiency Gas Turbine Action F: Gas Power Generation", funded under the "Energy, Environment and Sustainable Development" Programme, Contract N: NNE5/2001/382.

PRECCINSTA "Prediction and Control of Combustion Instabilities in Turbular und Annular GT Combustion Systems" funded under the "Energy, Environment and Sustainable Development" Programme, Contract N: ENK5/CT/2000/00 060.

The support through each of these projects is gratefully acknowledged.

Also, we would like to acknowledge the efforts by R. Borath of DLR's Institute of Materials Research in providing the micrographs of the seeding materials.

References

[1] C. Willert, M. Jarius: Planar flow field measurements in atmospheric and pressurized combustion chambers, Exp. Fluids **33**, 931–939 (2002) 286, 287, 289, 293, 294

[2] W. Kosiwczuk, A. Cessou, M. Trinité, B. Lecordier: Simultaneous velocity field measurements in two-phase flows for turbulent mixing of sprays by means of two-phase PIV, Exp. Fluids **39**, 895–908 (2005) 286, 306

[3] W. Kosiwczuk, A. Cessou, M. Trinité, B. Lecordier: Simultaneous measurements of gas and droplet velocity fields for turbulent mixing of GDI sprays by mean of two-phase PIV, in *13th Int. Symp. on Applic Laser Techniques to Fluid Mechanics* (2006) 286, 306

[4] C. Willert, B. Stasicki, M. Raffel, J. Kompenhans: A digital video camera for application of particle image velocimetry in high-speed flows, in *5th Int. Symposium on Optical Diagnostics in Fluid and Thermal Flows*, Proc. SPIE **2546** (1995) pp. 124–134 286

[5] D. Honore, S. Maurel, A. Quinqueneau: Particle image velocimetry in a semi-industrial 1 MW boiler, in *4th Int. Symp. on Particle Image Velocimetry* (2001) 287

[6] M. Fischer, G. Stockhausen, J. Heinze, M. Seifert, M. Müller, R. Schodl: Development of Doppler global velocimetry (DGV) measurement devices and combined application of DGV and OH*-chemiluminescence imaging to gas turbine combustor, in *12th Int. Symp. Applic Laser Techniques to Fluid Mechanics* (2004) 287, 303

[7] F. F. J. Schrijer, F. Scarano, B. W. van Oudheusden: Application of PIV in a Mach 7 double-ramp flow, Exp. Fluids **41**, 353–363 (2006) 288, 291

[8] W. D. Urban, M. G. Mungal: Planar velocity measurements in compressible mixing layers, in *35th Aerospace Sciences Meeting*, AIAA Paper 97-0757 (1997) 288

[9] J. H. Wernet, M. P. Wernet: Stabilized alumina/ethanol colloidal dispersion for seeding high temperature air flows, in *ASME Symp. on Laser Anemometry: Advances and Applications* (19–23 June 1994) 288

[10] C. Willert, C. Hassa, G. Stockhausen, M. Jarius, M. Voges, J. Klinner: Combined PIV and DGV applied to a pressurized gas turbine combustion facility, Meas. Sci. Technol. **17**, 1670–1679 (2006) 289, 293, 304, 305

[11] O. Diers, D. Schneider, M. Voges, P. Weigand, C. Hassa: Investigation of combustion oscillations in a lean gas turbine model combustor, in *ASME Turbo Expo 2007 - Power for Land, Sea and Air,* (2007) pp. GT2007–27360 293

[12] F. Güthe, B. Schuermans: Phase-locking in post-processing for pulsating flames, Meas. Sci. Technol. **18**, 3036–3042 (2007) 299, 302

[13] N. E. Huang, Z. Shen, S. R. Long, M. C. Wu, H. H. Shih, Q. Zheng, N.-C. Yen, C. C. Tung, H. H. Liu: The empirical mode decomposition and the Hilbert spectrum for nonlinear and non-stationary time series analysis, Proc. Royal Society A **454**, 903–995 (1998) 302

[14] N. E. Huang, M.-L. C. Wu, S. R. Long, S. S. P. Shen, W. Qu, P. Gloersen, K. L. Fan: A confidence limit for the empirical mode decomposition and Hilbert spectral analysis, Proc. Royal Society A **459**, 2317–2345 (2003) 302

[15] C. Hassa, C. Willert, M. Fischer, G. Stockhausen, I. Roehle, W. Meier, L. Wehr, P. Kutne: Nonintrusive flowfield, temperature and species measurements on a generic aeroengine combustor at elevated pressures, in *ASME Turbo Expo – Power for Land, Sea, and Air* (2006) pp. GT2006–90213 302, 303, 304
[16] M. P. Wernet: Planar particle imaging Doppler velocimetry: A hybrid PIV/DGV technique for three-component velocity measurements, Meas. Sci. Technol. **15**, 2011–2028 (2004) 303
[17] R. Schodl, I. Röhle, C. Willert, M. Fischer, J. Heinze, C. Laible, T. Schilling: Doppler global velocimetry for the analysis of combustor flow, Aerosp. Sci. Technol. **6**, 481–493 (2002) 303
[18] R. Schodl, G. Stockhausen, C. Willert, J. Klinner: Komplementär-Streifen-Verfahren für die Doppler Global Velocimetry (DGV) zur Korrektur des Einflusses von Hintergrundstrahlung, in *14. Fachtagung d. GALA (German Association for Laser Anemometry)* (2006) 306

Index